
MODEL ARCHITECTURE ADAPTION FOR BAYESIAN NEURAL NETWORKS

A PREPRINT

Duo Wang *
University of Cambridge
wd263@cam.ac.uk

Yiren Zhao *
University of Cambridge
yiren.zhao@cl.cam.ac.uk

Ilia Shumailov
University of Cambridge
ilia.shumailov@cl.cam.ac.uk

Robert Mullins
University of Cambridge
robert.mullins@cl.cam.ac.uk

ABSTRACT

Bayesian Neural Networks (BNNs) offer a mathematically grounded framework to quantify the uncertainty of model predictions but come with a prohibitive computation cost for both training and inference. In this work, we show a novel network architecture search (NAS) that optimizes BNNs for both accuracy and uncertainty while having a reduced inference latency. Different from canonical NAS that optimizes solely for in-distribution likelihood, the proposed scheme searches for the uncertainty performance using both in- and out-of-distribution data. Our method is able to search for the correct placement of Bayesian layer(s) in a network. In our experiments, the searched models show comparable uncertainty quantification ability and accuracy compared to the state-of-the-art (deep ensemble). In addition, the searched models use only a fraction of the runtime compared to many popular BNN baselines, reducing the inference runtime cost by $2.98\times$ and $2.92\times$ respectively on the CIFAR10 dataset when compared to MCDropout and deep ensemble.

1 Introduction

Deep Neural Networks (DNNs) are prone to over-fitting and often tend to make overly confident predictions Kristiadi et al. [2020], especially with inputs that are out of the original training data distribution. Ideally, we would like to have a principled DNN that assigns low confidence scores to samples that cannot be well interpreted from the training information and high scores to inputs that are in the training manifold. The ability for DNNs to say how certain they are in their predictions is particularly important for applications involving critical decision makings, such as healthcare and finance Jiang et al. [2017].

Bayesian Neural Networks (BNNs) offer a way to quantify uncertainty by approximating the posterior distribution over their model parameters. The general framework is to construct or re-form a stochastic component in the network, *e.g.* stochastic weights Blundell et al. [2015] or stochastic activations Gal and Ghahramani [2016], to simulate the effect of having multiple models θ with their associated probability distribution $q(\theta)$. When using a BNN for prediction, a set of possible models θ_i is sampled and is used to produce a set of output values that can later be aggregated to provide an uncertainty metric Jospin et al. [2020]. Naturally, at test time, this Monte-Carlo approach requires multiple BNN inference runs for a single input data point, causing a huge inference runtime overhead when considering deploying them into real production systems.

A practical approach to alleviating the runtime overhead is to adjust the BNN network architecture. For instance, it is popular to apply Bayesian inference on the (n -)last layer(s) only, this is equivalent to having a point estimate network followed by a shallow BNN Jospin et al. [2020]. Moreover, the architecture modifications can include other design dimensions in the network architecture design space, including channel lengths, kernel sizes, *etc.* This prompts the

*equal contribution

following question: *How can we automatically optimize BNN model architectures for both accuracy and uncertainty measurements?*

In this work, we demonstrate a novel network architecture search (NAS) algorithm that optimizes not only the in-distribution (i.d) data accuracy but also uncertainty measurements for both i.d and out-of-distribution (o.o.d) data. In particular, this work has the following contributions:

- We propose a novel network architecture search framework focusing on both accuracy and uncertainty measurements. Classic NAS optimizes solely for in-distribution likelihood, on the contrary, the proposed optimization framework searches for suitable architectures with the best uncertainty performance using both i.d and o.o.d data. We also propose a principled way of generating o.o.d data for NAS using Variational Auto-Encoders.
- We define a new search space for BNNs. The searched network can have a subset of layers (n -last layers) being stochastic while having the rest of the network being deterministic. We demonstrate how this design helps networks to achieve a better runtime when performing Bayesian inference.
- We empirically evaluate our method on multiple datasets and a wide collection of out-of-distribution data. Our experimental results outperform popular BNNs with fixed architectures and demonstrate comparable performance to deep ensembles but with significantly less runtime.

2 Background

2.1 Bayesian deep learning

It is well-known that an exact computation of the posterior distribution over model parameters of a modern Deep Neural Network is intractable. Bayesian Deep Learning methods rely on the mean-field assumption and Variational Bayes then allows us to find a distribution that approximates the true untractable posterior Graves [2011], Kingma and Welling [2013]. Blundell et al. proposed Bayes-by-Backprop, and their stochastic weights can be reparameterized as deterministic and differentiable functions. Gal and Ghahramani used a spike and slab variational distribution to reinterpret Dropout Srivastava et al. [2014] as approximate variational Bayesian inference. Osawa et al. proposed to use natural-gradient Variational Inference to perform Bayesian Learning and demonstrated that Bayesian Learning is possible on larger datasets Osawa et al. [2019]. There are also recent advances in Bayesian Deep Learning that turns noisy optimization to Bayesian inference Zhang et al. [2019], Maddox et al. [2019].

A typical Bayesian inference (using a BNN to run model inference) requires a Monte-Carlo estimate of the marginal likelihood of the posterior ($p(\hat{y}|\hat{x})$):

$$\mathbb{E}_{p(\hat{y}|\hat{x})} \approx \frac{1}{N} \sum_{n=0}^{N-1} f(\hat{x}, \theta_n) \quad (1)$$

(\hat{x}, \hat{y}) represents the test data point and f is a neural network parameterized by θ_n . The above formulation requires N samples and thus running model inference N times. This formulation is the key component for providing us with the model uncertainty measurements but also introduces a significant runtime overhead. In addition, as these Bayesian Learning methods rely on the mean field assumption, this comes at the cost of reduced expressivity. In the field of model uncertainty measurements, canonical methods such as deep ensemble offer the best performance but also suffer from the above-mentioned inference overhead, in addition, ensemble models also have a significant training overhead Lakshminarayanan et al. [2016].

Another piece of work, Bayesian subnetwork inference Daxberger et al. [2021], shares a similar motivation to us; they suggest that a full BNN’s uncertainty measurement capability might be well-preserved by a smaller sub-network from the original BNN. However, this proposed method does not provide any runtime reductions on GPUs as it still requires a Monte-Carlo based sampling over the full network as mentioned above.

Our NAS method is heavily inspired by Variational Inference based Bayesian Learning. In the experiments, we use Bayes-by-Backprop and MCDropout as the Bayesian baselines. More importantly, since the deep ensemble is seen as the state-of-the-art in model uncertainty calibration Jospin et al. [2020], with normally better or on par to Bayesian-based approaches, we will majorly focus on a comparison to it in our later evaluation.

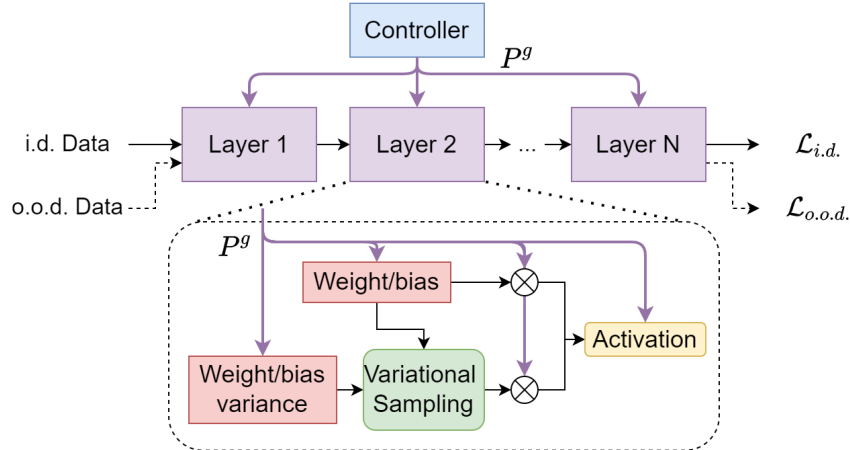


Figure 1: An overview of the Bayesian NAS framework. Controller outputs selection probability P^g for candidate operators in each layer of the template network. For Bayesian layers, additional variance parameters are also selected with P^g for variational sampling of weights. Controller selects the layer to be Bayesian or non-Baeyasian with trainable scaling variables. The search is optimized both for the in-distribution (i.d.) data loss $\mathcal{L}_{i.d.}$ and out-of-distribution (o.o.d) data loss $\mathcal{L}_{o.o.d}$ (Equation 4).

2.2 Network architecture search

There are now two major directions in the field of NAS, namely Gradient-based and Evolutionary-based NAS methods. Gradient-based NAS optimizes several pre-defined, trainable probabilistic priors Liu et al. [2018], Casale et al. [2019], Zhao et al. [2020a,b] and each scalar in these priors is associated with a pre-defined operation. The probabilistic priors are then updated using standard Stochastic Gradient Descent. Evolution-based NAS, on the other hand, operates on top of a pre-trained super-net and uses a search to rank the sub-network performances Cai et al. [2018, 2019], Zhao et al. [2021]. In this work, we follow the direction of Gradient-based NAS. We include a new formulation to optimize the network architectures using o.o.d data and also consider a new NAS optimization objective that is the uncertainty calibration.

Since the NAS problem can be viewed as a guided search that relies on prior observations, there is then a natural motivation to apply Bayesian Learning or Bayesian Optimization on NAS Zhou et al. [2019], White et al. [2019]. Our implemented NAS algorithm, however, has a very different motivation from this line of work.

3 Method

Figure 1 shows an overview of our Bayesian NAS framework. Our search framework contains a Bayesian template network (in purple) and a NAS controller (in blue). The Bayesian template network consists of stacks of layers of Bayesian and non-Bayesian candidate components. The choices of whether using a Bayesian or non-Bayesian layer, the activation functions, channel expansion counts, and kernel sizes together provide us a search space. During the search process, the NAS controller outputs selections of the candidate components of each layer in the template network. The layers with selected components are then assembled into a Bayesian model to process input data. We formulate the problem of searching for the best candidate network as a bi-level optimization, similar to typical gradient-based NAS strategies such as DARTS Liu et al. [2018] using trainable scaling variables. However what differentiates our Bayesian NAS from other NAS methods is that *we not only search in the classic NAS search space optimizing for in-distribution likelihood (usually categorical cross entropy for classification or Mean Squared Error for regression) but also have to search for the uncertainty performance using both in- and out-of-distribution data*. We propose a novel way of generating out-of-distribution data using Variational Auto-Encoders (VAEs) Kingma and Welling [2013] for NAS algorithms. In the following subsections, we discuss the search space, the NAS controller, our out-of-distribution data generation, and the dual optimization objectives in detail.

3.1 Search space

Table 1 illustrates a typical search space of each layer of the Bayesian template network for MNIST. We search over the expansion factors of the channel size (a.k.a a number of hidden units), the type of activation functions, and whether the

Table 1: Search space of each layer of the Bayesian template network for MNIST. Other search spaces are presented in our Appendix. ResNet18-based template has different channel expansion search options due to the limitation on GPU memory.

Search candidates	Possible options
Channel Expansion	0.5, 1, 1.5, 2, 4, 6, 8
Activation functions	ReLU, ELU, SELU, Sigmoid, ReLU6, LeakyReLU
Layer type	Non-bayesian, Bayesian
Kernel Size	1, 3, 5

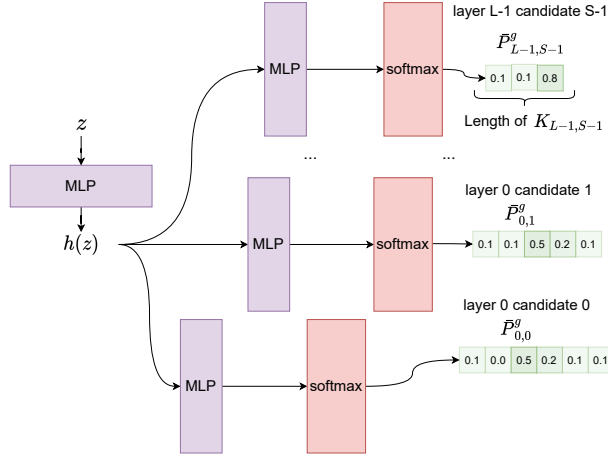


Figure 2: An overview of the NAS controller, where a trainable embedding z produces a set of output probability vectors $\bar{P}_{l,s}^g$. $\bar{P}_{l,s}^g$ vectors are then utilized to pick candidate operations from the search space.

layer is a Bayesian layer. If the layer is a Bayesian layer, we use candidate weight parameters as the mean for variational sampling, and additionally, search over candidate matrices of weights’ variances of the same shape as the weights’ mean Blundell et al. [2015]. For convolutional layers, we additionally search over the kernel size of the convolution kernels. Mathematically, we consider a Bayesian template network with L layers and the number of possible search candidates in each layer is S . For example, we have $S = 4$ in Table 1 (4 different search candidates). In a single layer presented in Table 1, the possible search options are $6 \times 6 \times 2 \times 3 = 216$ across these 4 search candidates for convolutional layers and 72 for linear layers (excluding the need of search for the kernel size).

For image classification tasks, we choose convolutional neural networks as our template networks. For MNIST dataset, we use a template network based on LeNet5 LeCun et al. [1998]. For CIFAR-10, our template network is ResNet18 He et al. [2016]. The search spaces for MNIST and CIFAR10 then have slight differences due to GPU memory limits. The search space and details of these search backbones are described in Appendix A.

The possible search space of the template network is large for even the simple LeNet5-based architectures containing 2 convolutional layers and 3 linear layers. This template network provides $216^2 * 72^3 \approx 10^8$ possible combinations, which is infeasible to traverse manually.

3.2 NAS controller

At each search iteration, the NAS Controller outputs selection probabilities $\bar{P}_{l,s}^g$ (named as P^g in Figure 1 for simplicity) for possible search candidates s for the l th layer of the template network. The NAS controller is conditioned on trainable free variables z such that it can model the joint distribution of the search options in all layers as $\bar{P}_{l,s}^g = P(l, s|z)P(z)$. In implementation we first embed z with an Multi-Layer Perception (MLP) into $h(z)$. For S possible search candidates and a network with L layers, we then have to output $L \times S$ probability vectors. The details and dimensions of these MLPs are included in Appendix B, we use $f_{l,s}$ to represent another MLP that produces the output probability vector:

$$\bar{P}_{l,s}^g = softmax(f_{l,k}(h(z))) \tag{2}$$

As illustrated in Figure 2, the probability vector $\bar{P}_{l,s}^g$ has a length of $K_{l,s}$ to represent selection probabilities for each of the $K_{l,s}$ candidates. To improve memory efficiency during the search, at each iteration we only select one candidate to be active for forward and backward pass, achieved via the argmax function. This is also known as the single-path search strategy in previous NAS frameworks Stamoulis et al. [2019]. By modeling the joint distribution $\bar{P}_{l,k}^g$ rather than the distribution for all possible (l, s) pairs as $P(l, s)$, we further reduce the computational and memory complexity from $O(\sum_{l=0, s=0}^{L-1, S-1} K_{l,s}^{LS})$ to $O(\sum_{l=0, s=0}^{L-1, S-1} LSK_{l,s})$.

In experiments, we found that the probability distribution can occasionally greedily converge to poor local minima due to a lack of exploration of the search space. In order to force the controller to explore rather than exploiting the randomness of training, we use additional noise to encourage exploration. In practice, we found that noise with Gaussian distribution truncated to be both positive works well. We anneal the noise level linearly with a slope (λ_n) after a preset warmup epoch (M_w). We pick the parameters of the noise annealing based on a hyperparameter study on the MNIST dataset as shown in Appendix C ($\lambda_n = 0.1, M_w = 20$).

3.3 Out-of-Distribution data generation

In previous Bayesian learning work Hafner et al. [2020], Daxberger et al. [2021], out-of-distribution data is generated by directly adding noise or performing a randomized affine transformation on input data. These methods, while able to generate out-of-distribution data, have a limited degree of freedom. In this work, we propose to first learn a latent probability distribution of the data using VAEs, and add noise in the latent space to generate out-of-distribution data. In this way, the degree of freedom is as high as what the generator neural network can model.

Typically, in a VAE, an encoder neural network embeds a datapoint x to a latent distribution $N(\mu_x, \sigma_x)$ with a mean μ_x and a standard deviation σ_x . We then sample $z \sim N(\mu_x, \sigma_x)$ and the decoder network produces a reconstructed x taken z as an input Kingma and Welling [2013, 2019]. In our formulation, we introduce another parameter β so that the sampling occurs as $z \sim N(\mu_x, \beta + \sigma_x)$. In other words, β controls the strength of the out-of-distribution data generation. A larger β value means data generated from the VAE would be more ‘out-of-distribution’.

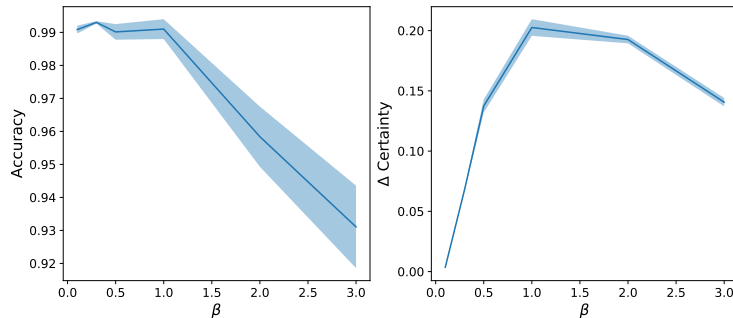


Figure 3: The effect of changing β when generating the o.o.d data utilized in the proposed NAS algorithm. The first plot shows the accuracy of the searched model on MNIST and the second plot shows the differences of model prediction certainties between i.d (test data of MNIST) and o.o.d (FashionMNIST) data. Results are averaged across three independent runs.

Table 2: The effect of VAE generated o.o.d data on MNIST. $\beta = 0.0$ would generate i.d data for NAS optimization. Both Without VAE and $\beta = 0.0$ give limited uncertainty quantifying abilities, *i.e.* the model cannot distinguish between i.d (MNIST data) and o.o.d data (FashionMNIST) with a small Δ Certainty gap (bigger is better).

Method Params	Without VAE	With VAE $\beta = 0$	With VAE $\beta = 1.0$
Accuracy	0.9923	0.9908	0.9910
Δ Certainty	0.0421	0.0036	0.2026

The network architectures and training strategies of our VAEs used on different datasets are included in our Appendix D. Figure 3 indicates a trade-off of different β values. A larger β value is often beneficial for the model to gain prediction certainty gaps between in- and out-of-distribution data. This means the model shows better performance and knows to be uncertain about data that is out-of-distribution. In the meantime, a large β value can hurt classification accuracy on

in-distribution data. Based on the results in Figure 3, we pick $\beta = 1.0$ for a balance between accuracy and certainty difference and use it for the rest of our evaluation.

To further demonstrate the effectiveness of using correctly generated o.o.d data in NAS, we present in Table 2 how the NAS performs without the VAE generated data, with incorrectly generated VAE data ($\beta = 0$) and a well-tuned o.o.d data ($\beta = 1.0$). Although all three approaches show similar accuracy metrics because of the NAS algorithm, well-tuned o.o.d data generation brings a significant performance boost when looking at the uncertainty measurements. Intuitively, when $\beta = 0$, the VAE generates i.d data for the NAS and does not contribute to uncertainty calibration.

3.4 Optimization

We formulate NAS as a bi-level optimization problem similar to DARTS Liu et al. [2018]:

$$\begin{aligned} \min_a \mathcal{L}_{val}(\theta^*(a), a) \\ \text{s.t. } \theta^*(a) = \arg \min_{\theta} (\mathcal{L}_{train}(\theta, a)) \end{aligned} \quad (3)$$

Here, θ are the parameters of all candidate operators, $\theta^*(a)$ is the optimal parameters given a , where a represents parameters of the architecture search controller a . L_{train} is a training loss on the training data split, while L_{val} is validation loss on the validation data split. The parameters θ and a are trained iteratively with their own optimizers. Since it is computationally intractable to compute $\theta^*(a)$ for each update of a , we approximate θ^* with a few training steps, which are shown to be effective in DARTS Liu et al. [2018].

For the training loss objective \mathcal{L}_{train} , we use corresponding likelihood objectives for different tasks (cross entropy for classification while MSE loss for regression). For the validation loss, in addition to the likelihood objective, we also include variance objectives for both the in-distribution and out-of-distribution data. The approximation of these variance objectives (using a variational distribution) is the same as the one utilized in Blundell et al., and a detailed discussion can be found in Jospin et al.. We minimize the validation set variances for in-distribution (i.d) data and maximize the variance for out-of-distribution (o.o.d) data (negative sign, and as illustrated in Figure 1). Therefore the validation loss becomes:

$$\mathcal{L}_{val} = \underbrace{\mathcal{L}_{likelihood}}_{\mathcal{L}_{i.d}} + \alpha \widehat{Var}_{i.d} - \underbrace{\gamma \widehat{Var}_{o.o.d}}_{\mathcal{L}_{o.o.d}} \quad (4)$$

Where $\mathcal{L}_{i.d}$ comprises likelihood and variance for i.d data, while $\mathcal{L}_{o.o.d}$ is the variance for o.o.d data. We consider $\alpha \in \{0.0001, 0.001, 0.01, 0.1\}$ and $\gamma \in \{0.0001, 0.001, 0.01, 0.1\}$. In practice we pick the α and γ values using only one epoch of training. We would like to make sure $\alpha \widehat{Var}_{i.d}$, $\gamma \widehat{Var}_{o.o.d}$ and $\mathcal{L}_{likelihood}$ are on the same level of magnitudes after an epoch of searching, so there is no overly dominant loss term that off-balances the optimization. In the implementation we found setting both α and γ to 0.01 often satisfies the above requirement, this type of control of α is also discussed in prior work on training Bayesian Neural Networks Blundell et al. [2015] (a.k.a KL re-weighting).

4 Experiments

We present our results with the following baselines on two image classification tasks, a loan approval prediction task and a heart disease prediction task.

- Point estimates or Non-Bayesian Neural Networks (Non-Bayesian): models trained with canonical Stochastic Gradient Descent and the network’s post-softmax outputs are used as a certainty metric.
- Bayes-by-Backprop networks with the local reparameterization trick (LRT): these models use unbiased Monte Carlo estimates to update the gradients Blundell et al. [2015].
- Monte-Carlo Dropout (MCDropout): this method makes the use of the Dropout layer Srivastava et al. [2014] to provide uncertainty measurements, where it can be interpreted as a less expressive inference compared to the Bayes-by-Backprop networks Gal and Ghahramani [2016].
- Deep Model Ensemble (Ensemble): this method does not use Bayesian inference but is normally seen as the state-of-the-art in uncertainty measurements Lakshminarayanan et al. [2016].

For all the baselines, we pick the best performing models trained with a set of learning rates $\{1e^{-2}, 1e^{-3}, 1e^{-4}\}$ and use a standard Adam optimizer Kingma and Ba [2014]. For any methods requiring a Monte-Carlo sampling, we use 10 samples for each approximation. In our experiment, we make sure each Deep Ensemble contains 10 models. In this case, the inference runtime of all baselines would be similar since all methods would have to perform 10 inference runs.

Table 3: MNIST, MNIST rotated, MNIST corrupted and FashionMNIST. Δ Certainty (bigger is better) shows the certainty gap compared to in-distribution data. NLL is the negative log-likelihood. Results are averaged across three independent runs.

Method	Non-Bayesian	LRT	MCDropout	Ensemble	NAS
MNIST (In distribution data)					
Accuracy	0.9902 ± 0.0008	0.9896 ± 0.0005	0.9342 ± 0.0061	0.9864 ± 0.0002	0.9910 ± 0.0011
Certainty	0.9984 ± 0.0003	0.9988 ± 0.0001	0.8965 ± 0.0585	0.9803 ± 0.0008	0.9951 ± 0.0020
NLL	0.2103 ± 0.0260	0.1001 ± 0.0014	0.7887 ± 0.0632	0.0458 ± 0.0018	0.0375 ± 0.0062
MNIST rotated 30 degrees (Out of distribution data)					
Accuracy	0.8663 ± 0.0102	0.8753 ± 0.0107	0.5954 ± 0.0352	0.8482 ± 0.0031	0.8545 ± 0.0059
Certainty	0.9752 ± 0.0032	0.9874 ± 0.0008	0.8896 ± 0.0617	0.8516 ± 0.0030	0.9475 ± 0.0164
NLL	3.4135 ± 0.1755	1.6534 ± 0.1239	22.9911 ± 12.5153	0.5163 ± 0.0085	0.7885 ± 0.1380
Δ Certainty	0.0232	0.0114	0.0068	0.1287	<i>0.0476</i>
MNIST corrupted level 1 (Out of distribution data)					
Accuracy	0.0992 ± 0.0039	0.0957 ± 0.0028	0.1066 ± 0.0038	0.1129 ± 0.0009	0.1009 ± 0.0016
Certainty	0.9755 ± 0.0254	0.8507 ± 0.0435	0.8334 ± 0.0736	0.7996 ± 0.0496	0.8438 ± 0.0827
NLL	10.0627 ± 0.8233	26.0908 ± 14.2407	34.0331 ± 14.2999	7.6489 ± 0.0380	13.6517 ± 5.3868
Δ Certainty	0.0147	0.1481	0.0630	0.1807	<i>0.1513</i>
FashionMNIST (Out of distribution data)					
Accuracy	0.0986 ± 0.0018	0.0973 ± 0.0006	0.1040 ± 0.0007	0.1058 ± 0.0007	0.0923 ± 0.0256
Certainty	0.9668 ± 0.0331	0.9538 ± 0.0422	0.8546 ± 0.0753	0.7011 ± 0.0396	0.7925 ± 0.0503
NLL	15.0814 ± 1.4024	32.1182 ± 16.4905	54.6312 ± 24.9626	5.4911 ± 0.2160	12.6002 ± 3.6958
Δ Certainty	0.0316	0.0450	0.0418	0.2792	<i>0.2026</i>
Inference Time with a batch size of 128 on NVIDIA GeForce RTX 2080 Ti (ms)					
Latency	12.0341 ± 0.5534	155.78073 ± 5.2058	102.7167 ± 2.0197	107.5535 ± 6.7008	<i>53.8164 ± 0.2321</i>

4.1 Image classification with distribution shifts

We consider two image classification tasks: MNIST Deng [2012] and CIFAR10 Krizhevsky et al. [2009], and include o.o.d datasets to examine the performance of the models with data distribution shifts:

- MNIST rotated 30 degrees: it contains all images in the test set of MNIST rotated by 30 degrees. Rotate 30 degrees is only considered as an o.o.d dataset for MNIST but not CIFAR10, because the training of the CIFAR10 model utilizes a random rotation augmentation.
- MNIST/CIFAR10 corrupted level n : we use corruptions introduced by Michaelis et al. with their openly available library. The corruptions are divided into n levels, where the higher n values indicate a more severe corruption. The corruptions are applied on the test partition of the datasets.
- FashionMNIST: Fashion-MNIST is a dataset of Zalando’s images, we use its test set that contains 10,000 examples to serve as an o.o.d dataset for MNIST Xiao et al. [2017].
- Street View House Numbers (SVHN): SVHN is a real-world image dataset for recognizing digits and numbers in natural scene images, we use its test set as an o.o.d dataset for CIFAR10 Netzer et al. [2011].

We use the hyper-parameters decided from Section 3, which we also summarize again here: $M_w = 20$, $\lambda_n = 0.1$ (Section 3.2); $\beta = 1.0$ (Section 3.3); $\alpha = \sigma = 0.01$ (Section 3.4). There are also two learning rates, one for training the Bayesian template network and one for the NAS controller. Similar as the treatment to the baselines, we manually select the learning rates from $\{1e^{-2}, 1e^{-3}, 1e^{-4}\}$ (a discussion about learning rate selections is in Appendix F).

Table 3 shows how the proposed NAS algorithm performs compared to the baselines. the Δ Certainty row shows the difference in the certainty metrics between i.d and o.o.d data. All results are from three independent search and retrain runs. It is worth pointing out that during the search of the architecture, our algorithm has also never seen any of these o.o.d datasets listed in Table 3. The NAS algorithm shows the best accuracy on i.d data, in addition, it achieves the second-best uncertainty performance in Table 3 (*i.e.* has the second-best score in Δ Certainty).

On the CIFAR10 dataset, in Table 4, the NAS algorithm shows comparable accuracy to a range of baseline methods. Surprisingly, it then also demonstrates the best ability in quantifying uncertainty. We hypothesize the deep ensemble approach shows less dominant numbers on this dataset because of the increased task complexity – the number of models in the ensemble might have to increase with the increased task complexity. However, in our comparison, to make sure

Table 4: CIFAR10, CIFAR10 corrupted and SVHN. Δ Certainty (bigger is better) shows the certainty gap compared to in-distribution data. NLL is the negative log-likelihood. Results are averaged across three independent runs.

Method	Non-Bayesian	LRT	MCDropout	Ensemble	NAS
CIFAR10 (In distribution data)					
Accuracy	0.9184 ± 0.0008	0.9187 ± 0.0043	0.8708 ± 0.0110	0.9176 ± 0.0011	0.9143 ± 0.0233
Certainty	0.9922 ± 0.0004	0.9921 ± 0.0004	0.9671 ± 0.0013	0.9921 ± 0.0001	0.9843 ± 0.0011
NLL	0.7544 ± 0.0240	0.6541 ± 0.0449	1.2205 ± 0.1253	0.7304 ± 0.0161	0.7422 ± 0.0203
CIFAR10 corrupted level 1 (Out of distribution data)					
Accuracy	0.1098 ± 0.0086	0.1116 ± 0.0072	0.0977 ± 0.0019	0.1124 ± 0.0052	0.1011 ± 0.0079
Certainty	0.8829 ± 0.0707	0.8772 ± 0.0889	0.9076 ± 0.0125	0.8487 ± 0.0077	0.7899 ± 0.0171
NLL	15.8335 ± 7.2911	14.7672 ± 2.8791	18.8109 ± 2.5662	14.0338 ± 1.1402	14.7175 ± 1.0371
Δ Certainty	0.1092	0.1150	0.0595	<i>0.1434</i>	0.1944
CIFAR10 corrupted level 3 (Out of distribution data)					
Accuracy	0.0999 ± 0.0026	0.1005 ± 0.0026	0.0987 ± 0.0017	0.1009 ± 0.0006	0.1121 ± 0.0020
Certainty	0.8898 ± 0.1013	0.8493 ± 0.0773	0.9090 ± 0.0382	0.8349 ± 0.0463	0.7864 ± 0.0249
NLL	15.9620 ± 13.1737	13.6133 ± 3.3533	18.2715 ± 3.9940	11.9185 ± 0.9514	12.4533 ± 0.8312
Δ Certainty	0.1024	0.1428	0.0581	<i>0.1573</i>	0.1979
SVHN (Out of distribution data)					
Accuracy	0.1040 ± 0.0038	0.1128 ± 0.0017	0.1263 ± 0.0033	0.1094 ± 0.0017	0.1025 ± 0.0087
Certainty	0.9469 ± 0.0111	0.9437 ± 0.0124	0.9376 ± 0.0111	0.9477 ± 0.0026	0.7960 ± 0.0134
NLL	24.4307 ± 2.7540	23.8798 ± 3.6388	22.2501 ± 2.2782	26.6406 ± 1.3254	20.0216 ± 1.0278
Δ Certainty	0.0453	<i>0.0484</i>	0.0295	0.0444	0.1883
Inference Time with a batch size of 32 on NVIDIA GeForce RTX 2080 Ti (ms)					
Latency	10.9965 ± 0.4044	188.1846 ± 3.34016	102.1346 ± 6.6028	104.0347 ± 0.5535	<i>34.9785 ± 1.3234</i>

the deep ensemble will have a similar runtime to BNNs, we kept the number of models in a deep ensemble to be 10. In contrast, our search then has the ability to automatically adapt to increased difficulties by exploring the architectural design space and therefore shows the best uncertainty measurements.

Table 5: Results of Heart Disease UCI. The objective is to predict the presence of heart disease in the patient. Δ Certainty (bigger is better) shows the certainty metric gap between in- and out-of-distribution data. NLL is the negative log-likelihood. Results are averaged across three independent runs.

Method	F1 Score	AUROC	Certainty	Δ Certainty	NLL
In distribution data					
Non-Bayesian	0.9785 ± 0.0152	0.9792 ± 0.0147	0.9893 ± 0.0100	-	0.0821 ± 0.0771
LRT	0.9375 ± 0.0000	0.9375 ± 0.0000	0.9514 ± 0.0028	-	0.1316 ± 0.0132
MCDropout	0.9882 ± 0.0112	0.9877 ± 0.0117	0.9919 ± 0.0040	-	0.0377 ± 0.0454
Ensemble	0.9892 ± 0.0152	0.9896 ± 0.0147	0.9913 ± 0.0029	-	0.0649 ± 0.0502
NAS	0.9936 ± 0.0013	0.9918 ± 0.0230	0.9977 ± 0.0033	-	0.0000 ± 0.0000
Out of distribution data					
Non-Bayesian	0.6628 ± 0.0533	0.5143 ± 0.0157	0.9074 ± 0.0539	0.0819	1.6745 ± 0.3862
LRT	0.7697 ± 0.0087	0.5212 ± 0.0027	0.6982 ± 0.0077	0.1532	0.7795 ± 0.0112
MCDropout	0.6475 ± 0.0378	0.5198 ± 0.0184	0.8568 ± 0.0197	0.1351	1.3935 ± 0.1628
Ensemble	0.6735 ± 0.0170	0.5171 ± 0.0059	0.9186 ± 0.0037	0.1727	1.8723 ± 0.0336
NAS	0.5709 ± 0.1056	0.5109 ± 0.0118	0.8231 ± 0.1952	0.1746	9.0560 ± 2.1621

4.2 Inference efficiency

Table 3 and Table 4 also have a row that show the inference time of running these models. It is worth mentioning that the inference time is averaged across 300 runs to provide a faithful reading.

The proposed NAS algorithm assigns layers to be Bayesian from the last layer to the first. This means the network will always try to assign later layers in the network to be Bayesian Brosse et al. [2020], Zeng et al. [2018]. The intuition is that it might be redundant to perform uncertainty measurements using the entire BNN, which is also empirically observed in Daxberger et al.. Bayesian inference on the last few layers might be sufficient for uncertainty calibration. For instance, if a 5-layer network is selected to have 2 Bayesian layers, this means only the last 2 layers are Bayesian.

Table 6: Results of Loan Approval. The objective is to predict the whether a house loan is approved or not. Δ Certainty (the bigger the better) shows the certainty metric gap between in- and out-of-distribution data. NLL is the negative log-likelihood. Results are averaged across three independent runs.

Method	F1 Score	AUROC	Certainty	Δ Certainty	NLL
In distribution data					
Non-Bayesian	0.8087 ± 0.0070	0.6365 ± 0.0121	0.9222 ± 0.0073	-	1.3513 ± 0.0500
LRT	0.8146 ± 0.0097	0.5294 ± 0.0415	0.8031 ± 0.0173	-	0.6116 ± 0.0025
MCDropout	0.7679 ± 0.0204	0.5540 ± 0.0263	0.9079 ± 0.0036	-	1.4507 ± 0.1558
Ensemble	0.8454 ± 0.0000	0.6381 ± 0.0000	0.8024 ± 0.0040	-	0.5694 ± 0.0029
NAS	0.8298 ± 0.0074	0.6393 ± 0.0006	0.8715 ± 0.0022	-	0.6914 ± 0.1203
Out of distribution data					
Non-Bayesian	0.6041 ± 0.0794	0.5067 ± 0.0111	0.8891 ± 0.0897	0.0331	2.1252 ± 0.8270
LRT	0.6667 ± 0.0000	0.5000 ± 0.0000	0.7200 ± 0.0261	0.0831	0.8143 ± 0.0373
MCDropout	0.5706 ± 0.0990	0.4907 ± 0.0090	0.8950 ± 0.0724	0.0831	2.1458 ± 1.0629
Ensemble	0.6667 ± 0.0000	0.5000 ± 0.0000	0.7425 ± 0.0137	0.1599	0.8553 ± 0.0187
NAS	0.6332 ± 0.0074	0.5032 ± 0.0021	0.6879 ± 0.0310	0.1836	0.7679 ± 0.0201

In this way, we have the ability to freeze the intermediate results after computing the first 3 layers, the later 2 layers can then use Bayesian inference to build a posterior estimation for the output. As a result, both of Table 3 and Table 4 show that the searched models are significantly faster than the baselines that have all layers being Bayesian.

Prior work has also demonstrated the use of Bayesian inference only on the (n -)last layer(s) only, intuitively, this approach can be seen as learning a point estimate transformation followed by a shallow BNN Jospin et al. [2020]. The user, however, has to determine which n last layer(s) is/are Bayesian by hand on a fixed architecture. Figure 4 shows how this manually designed last layer(s) only Bayesian approach (blue line) compares to our searched method (orange dot). The elaborated search space helps NAS to outperform the (n -)last layer(s) baselines by a significant margin. We present more data and detail in Appendix E.

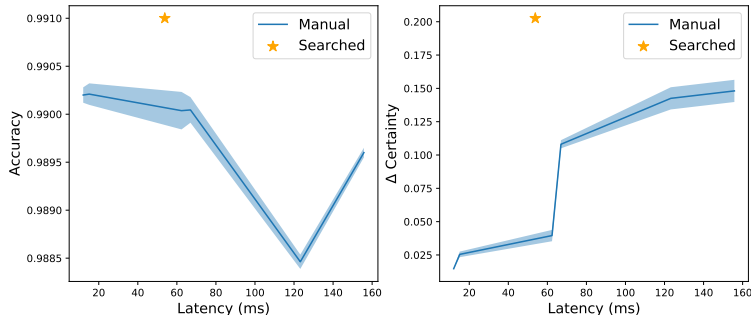


Figure 4: Latency vs. Accuracy and Latency vs. Δ Certainty tradeoffs. The blue line shows a Bayesian Neural Network, trained with LRT, with Bayesian inference on the (n -)last layer(s) only for MNIST classification. The searched network (orange star) greatly outperforms the manual baseline. Results are averaged across three independent runs and latency is measured on NVIDIA GeForce RTX 2080 Ti GPUs with a batch size of 128.

4.3 Potential applications with uncertainty measurements

In this section, we consider more realistic classification tasks (*e.g.* medical and financial tasks) that might be beneficial from having an uncertainty measurement. In these tasks, prevention of rare yet costly mistakes should normally be provided, in particular, we consider:

- Heart Disease HCI: This database contains 14 attributes to describe the conditions of a patient, the task is to classify whether the patient has potential heart diseases, this dataset is from the UC Irvine Machine Learning Repository Asuncion and Newman [2007]. All features are manually normalized.
- Loan Approval Prediction: This dataset contains 12 useful features about a customer applying for a house loan, the task is to predict whether the applicant is eligible for the loan Kaggle. All features are manually normalized.

- Out of distribution data: we generate o.o.d data for these datasets by using random features (white noise).

In both Table 5 and Table 6, our NAS generates results with high F1 scores (the best in Heart Disease HCI and the second-best in Loan Approval). In addition, the searched models show the best Δ Certainty on both datasets. The details about the network architectures for both the baselines and our search template model are in Appendix A. Inference time is not discussed in this case, since the runtime on small datasets is not likely to be a bottleneck in today’s systems.

On these simpler classification tasks, we see that our NAS algorithm outperforms the deep ensemble. We hypothesize that NAS algorithms are more advantageous on simple datasets. Intuitively, since these two tasks are significantly easier, the NAS method now contains a search space that has more possible models that will perform well. The NAS becomes an easier problem because there are now more equivalently good architectures for the algorithm to converge to.

On the other hand, we use Table 5 and Table 6 to demonstrate the effectiveness of the NAS method on applications that involve critical decision making and how NAS algorithm can help BNNs to achieve significantly better performance compared to BNNs with fixed architectures.

5 Conclusion

In this paper, we demonstrate a network architecture search method that can help Bayesian Neural Networks to find a suitable network architecture based on the targeting dataset. The proposed NAS method searches for architectures with not only the best accuracy but also a well-tuned certainty metric. The proposed method, unlike existing NAS approaches, makes use of both i.d and o.o.d data to achieve its optimization targets.

Empirically, we demonstrate that our NAS method can achieve comparable accuracy and uncertainty calibration compared to the deep ensemble on MNIST and CIFAR10. More importantly, the searched model can reduce the runtime by around $3\times$ compared to various BNN baselines and the deep ensemble.

A Baseline networks, NAS backbones and their search spaces

In Table 1, we illustrate a typical search space for MNIST. The only component of the search space that is different are the expansion factors. This is mainly because of the GPU memory limitation. For CIFAR10, the expansion factors are $\{0.5, 1, 1.5, 2, 2.5, 3.0, 3.5\}$ to ensure there is no Out-of-Memory error.

The Bayesian template network can have different structures. We use a LeNet5 based structure for problems on MNIST LeCun et al. [1998], and the ResNet-based structures He et al. [2016] is used on CIFAR10 classification. Table 7, Table 8 and Table 9 show the backbones used to construct the Bayesian template network used in our NAS. These backbone structures are also the network structures we used to construct other BNN baselines.

Table 7: Details of the LeNet5 NAS backbone

Layer Name	Base channel counts	Stride
Conv0	64	2
Conv1	64	2
Linear0	128	-
Linear1	128	-
Linear2	10	-

Table 8: Details of the MLP NAS backbone

Layer Name	Base channel counts	Stride
Linear0	32	-
Linear1	32	-
Linear2	32	-
Linear3	2	-

Table 9: Details of the ResNet-based NAS backbone

Layer Name	Base channel counts	Stride
Block0_Layer0	32	2
Block0_Layer1	32	1
Block0_Layer2	32	1
Block1_Layer0	64	2
Block1_Layer1	64	1
Block1_Layer2	64	1
Block2_Layer0	128	2
Block2_Layer1	128	1
Block2_Layer2	128	1
Block3_Layer0	256	2
Block3_Layer1	256	1
Block3_Layer2	256	1

B NAS controller MLP

As mentioned in Section 3.2, the NAS controller builds based on trainable embedding z that is then encoded using an MLP. The trainable free variable z is a vector of size 256 and we use a four-layer MLP with ReLU activations and 512 hidden units for each single layer. The output of the MLP is fed to multiple linear layers $f_{l,k}$ where the dimension of the layer will match the number of the possible candidates.

C Noise annealing for the NAS controller

As mentioned in Section 3.2, the NAS controller outputs a series of post-softmax vectors and pick suitable architectural operations based on these probabilities. Empirically, we found that adding noise to the post-softmax probabilities is

essential to avoid falling into local minima in the architecture search space. We used the following noise generation process:

$$p = \begin{cases} \lambda_n \times f_n(\mu = 0, \sigma = 1.0) & m \leq M_w \\ p_{softmax} + \lambda_n \times f_n(\mu = 0, \sigma = 1.0) \times (M_{total} - m) & otherwise \end{cases} \tag{5}$$

We found f_n can either be a Gaussian noise truncated to only contain the positive values or a log-normal distribution. In practice, we used the Gaussian noise with truncation. λ_n controls how aggressive the noise generation is and we linearly decrease the amount of noise after M_w number of epochs. m is the number of epoch and M is the total number of search epochs that is normally set to 100 in our experiments.

Figure 5 and Figure 6 show our hyper-parameter studies on different λ_n and M_w values. We then picked $\lambda_n = 0.1$, $M_w = 20$ for the best trade-off between accuracy and uncertainty performance. These two parameters together tunes the amount of exploration happens at the search stage. There should be an exploration for the NAS algorithm to avoid converge to local minima, but the exploration has to be limited so that finally the search process converges.

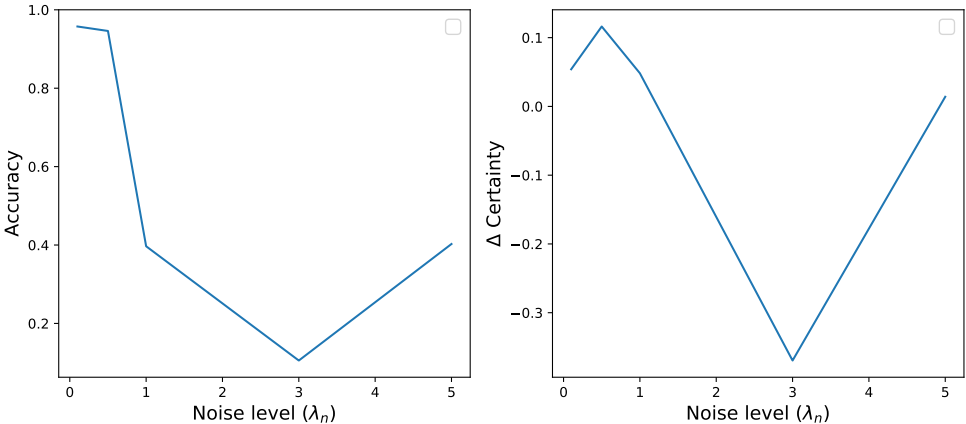


Figure 5: Accuracy and Δ Certainty tradeoffs with different noise levels (λ) used in the NAS controller on MNIST, with $N_{warmup} = 20$.

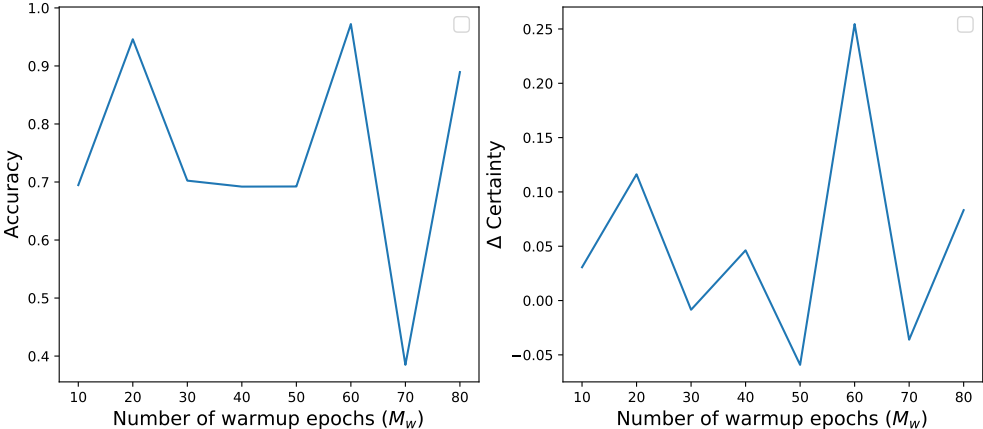


Figure 6: Accuracy and Δ Certainty tradeoffs with different number of warmup epochs (M_w) used in the NAS controller on MNIST, with $\lambda_n = 0.1$.

D VAE training setup

To generate o.o.d data, we use a VAE to embed the training dataset and produce a reconstructed, noisy o.o.d dataset.

We train the VAE for 100 epochs with standard data augmentations including random affine transformations and Gaussian noising where it is applicable. The VAE structure for Loan and Heart disease prediction contains a four-layer encoder, four-layer decoder architecture; each layer in this VAE contains 128 hidden units. The VAE used for image datasets (MNIST and CIFAR) contains four convolutional layers for encoder and four convolutional layers for decoder. Table 10 illustrates the model architecture of the VAE, and we use $n = 32$ for MNIST and $n = 64$ for CIFAR10. The binary cross entropy loss is used for image datasets, and Mean-squared-error loss is used for other prediction tasks. We found that an Adam optimizer with a learning rate of $1e^{-4}$ is suitable for training the VAE on various datasets.

Table 10: VAE model on the MNIST and CIFAR10 dataset, we use $n = 32$ for MNIST and $n = 64$ for CIFAR10. The final layer will have 3 channels for CIFAR10 and 1 channel for MNIST.

Layer Name	channel counts	Stride	Kernel size
Encode_Conv0	n	2	3
Encode_Conv1	$n \times 2$	2	3
Encode_Conv2	$n \times 4$	2	3
Encode_Conv3	$n \times 4$	2	3
Decoder_Deconv0	$n \times 4$	2	3
Decoder_Deconv1	$n \times 4$	2	3
Decoder_Deconv2	$n \times 2$	2	3
Decoder_Deconv3	3/1	2	3

E Bayesian inference on the n-last layer(s)

A common design practice to reduce the runtime overhead of BNNs is to only use the later portion of the network to perform Bayesian inference. While Section 4.2 discussed the inference efficiency difference between the NAS searched models and hand-designed models. In Figure 7 we illustrate the details of the hand-designed models. This plot shows how having different numbers of Bayesian layers can affect accuracy, uncertainty measurements and latency.

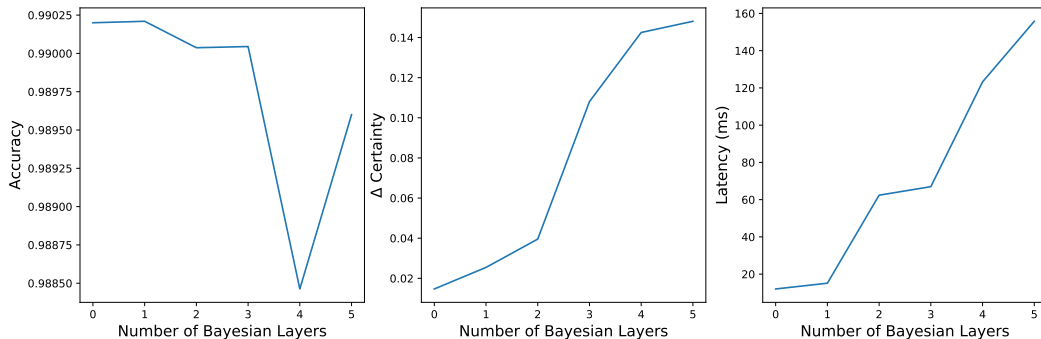


Figure 7: Accuracy Δ Certainty and Latency tradeoffs with different number of Bayesian layers on a Lenet5 based architecture with LRT.

F The effect of different learning rates

The NAS algorithm contains a bi-level optimization as mentioned in our main paper. We use two Adam optimizers to update the Bayesian template networks and the NAS controller respectively. There then exist two learning rates, one for training the backbone network (lr_t) and the other for the NAS controller lr_{arch} . As mentioned in Section 4, we pick the learning rates from $\{1e^{-2}, 1e^{-3}, 1e^{-4}\}$. Our results in Table 11 show that a suitable learning rate combination for our NAS algorithm is $lr_t = 1e^{-4}$, $lr_{arch} = 1e^{-3}$, we use this learning rate combination for all other datasets in the main paper.

Table 11: Running the NAS algorithm with different learning rates for MNIST classification, results are averaged across three independent runs. lr_t and lr_{arch} represent the learning rate for the Bayesian template network and the learning rate for the NAS controller respectively.

lr_{arch}	lr_t		
	$1e^{-2}$	$1e^{-3}$	$1e^{-4}$
$1e^{-2}$	0.3566 ± 0.0061	0.9689 ± 0.0008	0.9901 ± 0.0005
$1e^{-3}$	0.7728 ± 0.0391	0.9883 ± 0.0018	0.9910 ± 0.0011
$1e^{-4}$	0.8566 ± 0.0021	0.9733 ± 0.0002	0.9823 ± 0.0019

References

- Agustinus Kristiadi, Matthias Hein, and Philipp Hennig. Being bayesian, even just a bit, fixes overconfidence in relu networks. In *International Conference on Machine Learning*, pages 5436–5446. PMLR, 2020.
- Fei Jiang, Yong Jiang, Hui Zhi, Yi Dong, Hao Li, Sufeng Ma, Yilong Wang, Qiang Dong, Haipeng Shen, and Yongjun Wang. Artificial intelligence in healthcare: past, present and future. *Stroke and vascular neurology*, 2(4), 2017.
- Charles Blundell, Julien Cornebise, Koray Kavukcuoglu, and Daan Wierstra. Weight uncertainty in neural network. In *International Conference on Machine Learning*, pages 1613–1622. PMLR, 2015.
- Yarin Gal and Zoubin Ghahramani. Dropout as a bayesian approximation: Representing model uncertainty in deep learning. In *international conference on machine learning*, pages 1050–1059. PMLR, 2016.
- Laurent Valentin Jospin, Wray Buntine, Farid Boussaid, Hamid Laga, and Mohammed Bennamoun. Hands-on bayesian neural networks—a tutorial for deep learning users. *arXiv preprint arXiv:2007.06823*, 2020.
- Alex Graves. Practical variational inference for neural networks. *Advances in neural information processing systems*, 24, 2011.
- Diederik P Kingma and Max Welling. Auto-encoding variational bayes. *arXiv preprint arXiv:1312.6114*, 2013.
- Nitish Srivastava, Geoffrey Hinton, Alex Krizhevsky, Ilya Sutskever, and Ruslan Salakhutdinov. Dropout: a simple way to prevent neural networks from overfitting. *The journal of machine learning research*, 15(1):1929–1958, 2014.
- Kazuki Osawa, Siddharth Swaroop, Anirudh Jain, Runa Eschenhagen, Richard E Turner, Rio Yokota, and Mohammad Emteyaz Khan. Practical deep learning with bayesian principles. *arXiv preprint arXiv:1906.02506*, 2019.
- Ruqi Zhang, Chunyuan Li, Jianyi Zhang, Changyou Chen, and Andrew Gordon Wilson. Cyclical stochastic gradient mcmc for bayesian deep learning. *arXiv preprint arXiv:1902.03932*, 2019.
- Wesley J Maddox, Pavel Izmailov, Timur Garipov, Dmitry P Vetrov, and Andrew Gordon Wilson. A simple baseline for bayesian uncertainty in deep learning. *Advances in Neural Information Processing Systems*, 32:13153–13164, 2019.
- Balaji Lakshminarayanan, Alexander Pritzel, and Charles Blundell. Simple and scalable predictive uncertainty estimation using deep ensembles. *arXiv preprint arXiv:1612.01474*, 2016.
- Erik Daxberger, Eric Nalisnick, James U Allingham, Javier Antorán, and José Miguel Hernández-Lobato. Bayesian deep learning via subnetwork inference. In *International Conference on Machine Learning*, pages 2510–2521. PMLR, 2021.
- Hanxiao Liu, Karen Simonyan, and Yiming Yang. Darts: Differentiable architecture search. *arXiv preprint arXiv:1806.09055*, 2018.
- Francesco Paolo Casale, Jonathan Gordon, and Nicolo Fusi. Probabilistic neural architecture search. *arXiv preprint arXiv:1902.05116*, 2019.
- Yiren Zhao, Duo Wang, Xitong Gao, Robert Mullins, Pietro Lio, and Mateja Jamnik. Probabilistic dual network architecture search on graphs. *arXiv preprint arXiv:2003.09676*, 2020a.
- Yiren Zhao, Duo Wang, Daniel Bates, Robert Mullins, Mateja Jamnik, and Pietro Lio. Learned low precision graph neural networks. *arXiv preprint arXiv:2009.09232*, 2020b.
- Han Cai, Ligeng Zhu, and Song Han. Proxylessnas: Direct neural architecture search on target task and hardware. *arXiv preprint arXiv:1812.00332*, 2018.
- Han Cai, Chuang Gan, Tianzhe Wang, Zhekai Zhang, and Song Han. Once-for-all: Train one network and specialize it for efficient deployment. *arXiv preprint arXiv:1908.09791*, 2019.
- Yiren Zhao, Xitong Gao, Ilia Shumailov, Nicolo Fusi, and Robert Mullins. Rapid model architecture adaption for meta-learning. *arXiv preprint arXiv:2109.04925*, 2021.

- Hongpeng Zhou, Minghao Yang, Jun Wang, and Wei Pan. Bayesnas: A bayesian approach for neural architecture search. In *International Conference on Machine Learning*, pages 7603–7613. PMLR, 2019.
- Colin White, Willie Neiswanger, and Yash Savani. Bananas: Bayesian optimization with neural architectures for neural architecture search. *arXiv preprint arXiv:1910.11858*, 1(2), 2019.
- Yann LeCun, Léon Bottou, Yoshua Bengio, and Patrick Haffner. Gradient-based learning applied to document recognition. *Proceedings of the IEEE*, 86(11):2278–2324, 1998.
- Kaiming He, Xiangyu Zhang, Shaoqing Ren, and Jian Sun. Deep residual learning for image recognition. In *Proceedings of the IEEE conference on computer vision and pattern recognition*, pages 770–778, 2016.
- Dimitrios Stamoulis, Ruizhou Ding, Di Wang, Dimitrios Lymberopoulos, Bodhi Priyantha, Jie Liu, and Diana Marculescu. Single-path nas: Designing hardware-efficient convnets in less than 4 hours. *arXiv preprint arXiv:1904.02877*, 2019.
- Danijar Hafner, Dustin Tran, Timothy Lillicrap, Alex Irpan, and James Davidson. Noise contrastive priors for functional uncertainty. In *Uncertainty in Artificial Intelligence*, pages 905–914. PMLR, 2020.
- Diederik P Kingma and Max Welling. An introduction to variational autoencoders. *arXiv preprint arXiv:1906.02691*, 2019.
- Diederik P Kingma and Jimmy Ba. Adam: A method for stochastic optimization. *arXiv preprint arXiv:1412.6980*, 2014.
- Li Deng. The mnist database of handwritten digit images for machine learning research [best of the web]. *IEEE Signal Processing Magazine*, 29(6):141–142, 2012.
- Alex Krizhevsky, Geoffrey Hinton, et al. Learning multiple layers of features from tiny images. 2009.
- Claudio Michaelis, Benjamin Mitzkus, Robert Geirhos, Evgenia Rusak, Oliver Bringmann, Alexander S Ecker, Matthias Bethge, and Wieland Brendel. Benchmarking robustness in object detection: Autonomous driving when winter is coming. *arXiv preprint arXiv:1907.07484*, 2019.
- Han Xiao, Kashif Rasul, and Roland Vollgraf. Fashion-mnist: a novel image dataset for benchmarking machine learning algorithms. *arXiv preprint arXiv:1708.07747*, 2017.
- Yuval Netzer, Tao Wang, Adam Coates, Alessandro Bissacco, Bo Wu, and Andrew Y Ng. Reading digits in natural images with unsupervised feature learning. 2011.
- Nicolas Brosse, Carlos Riquelme, Alice Martin, Sylvain Gelly, and Éric Moulines. On last-layer algorithms for classification: Decoupling representation from uncertainty estimation. *arXiv preprint arXiv:2001.08049*, 2020.
- Jiaming Zeng, Adam Lesnikowski, and Jose M Alvarez. The relevance of bayesian layer positioning to model uncertainty in deep bayesian active learning. *arXiv preprint arXiv:1811.12535*, 2018.
- Arthur Asuncion and David Newman. Uci machine learning repository, 2007.
- Kaggle. Loan prediction. <https://www.kaggle.com/ninzaami/loan-predication>. Accessed: 2020-09-30.